

© IEEE. Personal use of this material is permitted. However, permission to reprint/republish this material for advertising or promotional purposes or for creating new collective works for resale or redistribution to servers or lists, or to reuse any copyrighted component of this work in other works must be obtained from the IEEE.

This material is presented to ensure timely dissemination of scholarly and technical work. Copyright and all rights therein are retained by authors or by other copyright holders. All persons copying this information are expected to adhere to the terms and constraints invoked by each author's copyright. In most cases, these works may not be reposted without the explicit permission of the copyright holder.

VALIDATION AND RELIABILITY OF THE DISCRIMINATIVE POWER OF GEOMETRIC WOOD LOG END FEATURES

Rudolf Schraml^a Alexander Petutschnigg^b Andreas Uhl^a

^a University of Salzburg, Jakob Haringer Str. 2, 5020 Salzburg, Austria

^b University of Applied Sciences Salzburg, Markt 136a, 5431 Kuchl, Austria

ABSTRACT

Recent investigations on biometric log recognition using end face images indicated that shape information is beneficial for the biometric system performance. This study assesses the discriminative power and reliability of geometric features which are computed by means of segmented cross-sections and their pith positions.

The experimental evaluation is based on cross-section images from 150 different logs, for which the ground truth of the boundary and pith position is known. By assessing the verification performance for ground truth data and automated segmentation/ pith estimation procedures this work highlights the basic discriminative power of geometric log end features and further validates their reliability in case of using automated procedures.

Index Terms— Geometric Log End Features, Biometric Log Traceability, Wood Log Cross-section Analysis

1. INTRODUCTION

Biometric tracking of wood logs is a potential approach to establish traceability without the necessity for physical markers like plastic badges or Radio Frequency Identification (RFID) transponders. A biometric log recognition system based on log end images could be used to track the ownership from the forest based industries to further processing companies. Another application is to discover illegally harvested tree logs based on cross-section (CS) images of their stumps [1].

In recent publications [2, 3] we have investigated the general applicability and robustness of a texture-feature based approach [4, 5] for a biometric log recognition system. The experiments were based on CS slices from three different logs and the results indicated a high degree of robustness to temporal, longitudinal and surface variations which arise in a real world application. Based on these findings we explored the applicability of fingerprint and iris-recognition based methods to identify 150 different tree logs in [6]. The best fingerprint-based approach utilized shape information in the matching procedure. Furthermore, the iris-based approaches

rely on polar-transformation which is based on the CS boundary and pith position. Basically, the results showed that shape information is required to achieve an acceptable verification and identification performance. So far, all experiments were conducted using ground truth (GT) data of the CS boundaries and pith positions.

The present study has the objective to assess the discriminative power of geometric log end features based on GT data and to validate their reliability in case of performing automated CS segmentation (SEG) and pith estimation (PE).

For the experiments the test set used in [6] is used and different geometric features are extracted based on the CS boundaries and pith positions. In assessing the verification performance for GT data this work investigates the basic discriminative power of these features. In validating the reliability of geometric features, for different configurations of SEG and PE approaches, this work contributes to the further development of a biometric log recognition system.

Section 2 introduces the utilized SEG and PE approaches. Subsequently, a set of geometric features based on the CS boundary and pith position is presented. The experimental setup and results are presented in Section 3 followed by the conclusion in Section 4.

2. GEOMETRIC LOG END FEATURES

The computation of geometric log end features relies on the boundary and the pith position of a CS. Furthermore, the pith position and CS boundary are required for any CS registration procedures. Scale and rotational variances can be compensated by rotating the CS around the pith position and scaling the CS to a certain size. Before describing a set of geometric log end features, we briefly introduce the utilized SEG and PE approaches.

2.1. Pith Estimation and CS Segmentation

PE is based on the assumption that local orientations of annual ring patches point into the direction of the pith. For this purpose, local orientation estimates are computed using two Fourier spectrum analysis approaches: Peak and Principal Component Analysis (PCA) as suggested in [7]. The image is subdivided into blocks and the intersections of their

local orientation estimates are summed up in an accumulator array. This array is smoothed with a Gaussian and the maximum intersection cell is used as pith estimate.

For SEG the pith position (either the GT or the PE result) is utilized as initial starting point for the similarity based region growing procedure suggested in [8]. Similar as for PE, the input image is subdivided into blocks. Four clusters, each consisting of four blocks, are initialized close around the pith position. The subsequent region growing procedure is based on intensity histogram distances between the blocks of a cluster which are computed using the Earth Movers Distance (EMD). Blocks along the cluster boundaries that fulfil the similarity criteria are added to each cluster until no more blocks can be added. Finally, the clusters are merged and the respective concave hull is utilized as SEG result.

2.2. Geometric Feature Extraction

Once the CS boundary and the pith position are determined several geometric features can be computed [9, p.323ff]. Fig. 1a illustrates an exemplary CS image and in Fig. 1b an overview of important geometric measurements is provided. Subsequently, the set of utilized features is presented. A_{CS} and P_{CS} give the area and perimeter of the CS and BB specifies the minimum bounding box.

HU Moments (H_{1-7}) = seven invariant image moments proposed by [10].

Zernike Moments (Z) = 10 orders of complex Zernike moments are computed for the CS shape [11, 12].

Circularity (C) = $4\Pi \cdot (A_{CS}/P_{CS}^2)$, describes how similar to a circle the CS is.

Rectangularity (R) = A_{CS}/A_{BB} , ratio between A_{CS} and the area of the minimum bounding rectangle (A_{BB}).

Eccentricity (E) = BB_W/BB_H , ratio between width and height of the minimum bounding box.

Pith Eccentricity (PEC) = distance between the centroid (CM) of the CS and the pith position (PP) normalized using the width of the BB_W .

Centroid distances (CD) = centroid (CM) to border distances per degree ($CD_\phi, \phi \in \{1^\circ, \dots, 360^\circ\}$) normalized by $\max CD_\phi$.

Pith distances (PD) = the pith to border distances per degree ($PD_\phi, \phi \in \{1^\circ, \dots, 360^\circ\}$) normalized by $\max PD_\phi$.

3. EXPERIMENTS AND RESULTS

The experimental setup is chosen to assess two questions. First, the general biometric performance of geometric features is assessed by using GT data. Second, we validate their reliability in case of different configurations for SEG and PE.

Testset: For the experiments the same test sets (TS_1, TS_2) as in [6] are utilized. TS_1 consists of 50 tree logs. Each log was captured four times with and without flash. To investigate

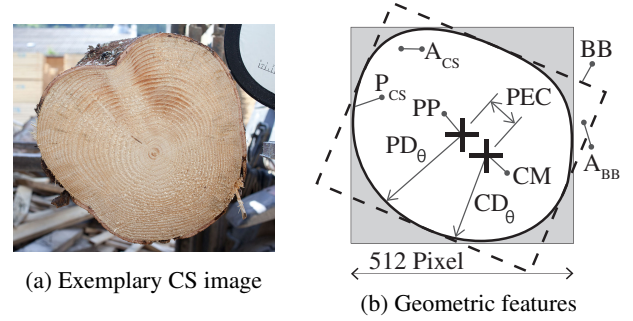


Fig. 1: Geometric feature extraction illustration.

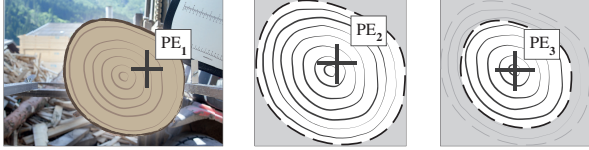
the impact of a clearance cut in the sawmill the ends of eight logs from TS_1 were cross-cut and captured once again, with and without flash. For TS_2 105 strongly bended logs were captured three times without flash. Commonly, bended logs show a high amount of reaction wood. This leads to elliptical shaped CSs. For each CS image the pith position and the CS border were determined manually.

Computational details For each CS image the CS boundary and pith position is determined using four different configurations. Two approaches for SEG and two for PE are utilized. For SEG these approaches distinguish in using grey value (SEG-G) or RGB histograms (SEG-C) for computing the EMD between two blocks. In case of PE the Peak (PE-PEAK) or PCA (PE-PCA) approach for local orientation estimation are utilized. For each configuration and the respective PE approach different variations for estimating the pith are assessed. The first variation (P_1) estimates the pith using local orientations computed from the entire image (see Fig. 3a). In the experiments P_1 is used as seed point for SEG. The second variation (P_2) is computed by just using local orientations within the CS boundary (see Fig. 3b). As shown in [7], local orientation estimates close to the pith are more circular and thus the third variation (P_3) is computed within the half-sized CS boundary. P_1, P_2, P_3 are computed using half-overlapping 16x16 pixels blocks. The fourth variation (P_4) is computed like P_3 with the difference that a block-overlapping factor of four is utilized.

Additionally, three variations are computed using a saw cut suppression mode. This mode computes the orientation



Fig. 2: 1st Row (TS_1): Respectively, two CS-Images from two different logs - one captured with flash and one without flash. 2nd Row (TS_2): Four CS-Images from different logs.



(a) PE within the total im- (b) PE within the (c) PE within the
age CS boundary scaled CS boundary

Fig. 3: Illustration of the pith estimation (PE) variations.

distribution for all local orientations in the considered region. If the most frequent orientation has a frequency remarkably higher than the mean plus two times the variance the corresponding magnitudes in all Fourier spectra are zeroed and the local orientation estimates are recomputed. The saw-cut suppressed PE variations are denoted as $P_{2SS}, P_{3SS}, P_{4SS}$.

For all configurations and the GT data the geometric features described in Section 2 are computed. For each feature the matching scores between all CS-Images of both testsets are computed and finally the matching scores are normalized.

3.1. Results

Initially, the verification performance of geometric features based on GT data (i.e. manually determined pith position and CS boundary) is assessed. The performance is assessed for each feature separately and for score level fusion [13, p.225] for different numbers (k) of features. These are determined using Selective Floating Forward Selection (SFFS) [14] which is configured to minimize the overlap between the inter- and intraclass distribution.

Second, the accuracies for the SEG/PE configurations and the PE variations are considered in detail. The most accurate PE variation is then utilized as pith estimate to evaluate the verification performance in case of automated SEG and PE. Basically, the verification performance is assessed considering the EER and margin of error (MOE) which is estimated for a 90% level of confidence using subset partitioning [15].

Groundtruth-based Verification Performance The results in Table 2 show that several features achieve respectable EERs. In case of E,PEC,RD,CD and Z the EERs are below 10%. The overall best EER is achieved using PD which shows an EER of 1.4%. In case of SFFS, the results in Table 1 show that the best result is achieved with (PD,CD,Z) EER=0.54%. Based on these results it can be stated that these features principally have a high discriminative power.

CS segmentation and pith estimation accuracy The SEG accuracy is specified by the F-Measure between the GT mask and the SEG result. The PE accuracy is given as the pixel distance between the GT and the estimated pith position. In Table 3 the mean and standard deviations for the accuracies of all configurations are summarized. SEG-C and SEG-G show a similar segmentation performance although there are big

SEG/PE	$k=2$	$k=3$	$k=4$
GT	PD,CD 0.74 ± 0.8	PD,CD,Z 0.54 ± 0.5	PD,CD,Z,R 0.68 ± 0.6
SEG-G/PE-PCA	PD,H_4 20.12 ± 2.4	PD,H_4,R 20.07 ± 2.6	PD,H_4,R,H_7 20.10 ± 2.3
SEG-G/PE-PEAK	PD,C 21.84 ± 2.8	PD,E,C 22.52 ± 3.2	PD,CD,E,C 23.28 ± 3.2
SEG-C/PE-PCA	PD,CD 15.75 ± 2.6	PD,CD,E 15.81 ± 3.1	PD,CD,E,H_6 15.88 ± 3.3
SEG-C/PE-PEAK	PD,CD 15.36 ± 3.4	PD,CD,R 15.34 ± 3.4	PD,CD,R,E 15.61 ± 3.1

Table 1: EER±MOE[%]: SFFS-based score level fusion. Z is not considered in case of SEG/PE.

differences when considering the particular results for each CS in detail. This can be observed for the P_2 results showing remarkable PE accuracy differences between the SEG-C and SEG-G configurations.

Overall PE results for SEG/PE the best accuracy is reached with SEG-G/PE-PEAK and P_{4SS} . The particular results are illustrated in Fig. 4. For each log end the mean, min. and max. accuracy for SEG and PE is depicted. The chart illustrates that the segmentation accuracies for TS_1 are better than for TS_2 . This is caused by the deformed CSs in TS_2 (see Fig. 2) which likely show reaction wood on their end faces. This observation is also visible for the PE accuracies which are better in case of TS_1 . Furthermore, it can be recognized that there is no direct relationship between SEG and PE accuracy.

However, the results show that for the GT-based configurations the P_2 and P_{2SS} variations achieve the best PE accuracies. In difference to the GT-based PE results, the accuracies for SEG-C and SEG-G using P_3 and P_4 are remarkably better. We assume that this is caused by the segmentation errors which influence the performance of P_2 and P_{2SS} . Due to down-scaling the CS border for P_3 and P_4 the probability of using wrong orientation estimates is reduced. In comparing the results for P_3 and P_4 to P_{3SS} and P_{4SS} the improved PE accuracy in case of sawcut suppression is recognizable.

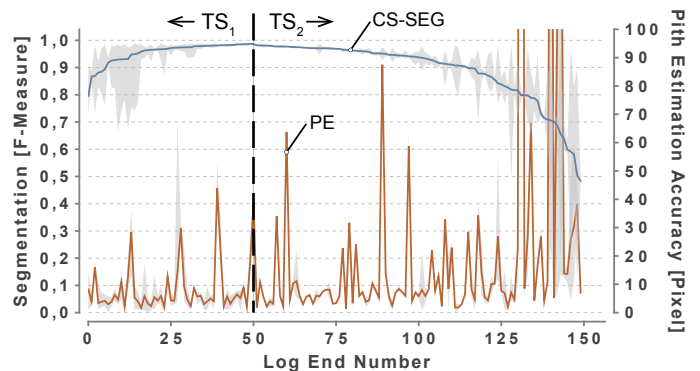


Fig. 4: Mean, min. and max. accuracies for SEG-G/PE-PEAK and P_{4SS} grouped by the images of each log end.

SEG/PE	HU ₁	HU ₂	HU ₃	HU ₄	HU ₅	HU ₆	HU ₇	C	R	E	PEC	CD	PD	Z
GT	11.6±3.1	13.8±3.4	19.7±3.9	25.1±4.5	30.7±5.5	28.2±5.9	29.5±5.3	17.4±5.0	22.1±4.2	8.1±1.8	7.2±1.2	2.8±2.4	1.4±0.7	6.3±1.2
SEG-G/PE-PCA	33.6±2.6	34.1±2.0	39.2±3.5	42.1±1.8	42.4±1.7	37.2±2.6	41.3±2.3	34.8±2.9	40.0±0.4	29.8±2.4	29.1±3.4	28.1±3.2	20.0±2.5	5.6±1.0
SEG-G/PE-PEAK	32.8±2.8	33.7±2.9	38.5±3.5	41.2±2.1	40.6±2.1	37.0±2.5	41.6±2.0	36.0±2.7	38.3±0.7	28.9±2.4	28.6±3.0	27.1±3.5	20.3±3.0	5.6±1.0
SEG-C/PE-PCA	29.7±2.1	31.8±1.9	36.5±3.8	41.7±1.5	44.2±1.2	35.6±2.3	40.6±2.0	29.1±3.2	36.3±2.1	24.0±2.5	27.6±2.9	20.3±3.4	16.6±2.8	5.5±1.1
SEG-C/PE-PEAK	31.0±2.6	32.0±2.6	36.6±3.5	40.6±1.5	41.2±1.3	36.3±2.0	40.3±1.8	30.5±3.1	36.7±0.8	24.1±2.5	26.2±2.9	19.4±3.4	15.2±2.8	5.4±1.0

Table 2: EER±MOE[%] for each geometric feature and all configurations.

SEG/PE	F-Measure	P ₁	P ₂	P _{2SS}	P ₃	P _{3SS}	P ₄	P _{4SS}
GT/PE-PCA	–	–	18.9±20.1	19.5±19.6	16.8±25.8	15.4±18.9	16.8±32.9	14.4±19.5
GT/PE-PEAK	–	–	13.2±24.9	11.5±14.5	20.2±33.3	21.3±32.0	19.7±35.9	22.1±38.4
SEG-G/PE-PCA	0.91±0.11	24.9±37.1	20.9±40.1	21.7±42.6	18.5±44.2	17.8±40.8	17.7±44.8	16.5±40.6
SEG-G/PE-PEAK	0.91±0.11	24.0±39.3	16.1±43.1	15.9±42.6	14.8±45.1	13.7±41.6	14.2±45.4	13.0±41.6
SEG-C/PE-PCA	0.93±0.10	24.9±37.1	22.0±45.3	23.0±47.6	19.0±44.2	17.8±40.4	17.6±44.2	17.1±42.5
SEG-C/PE-PEAK	0.93±0.10	24.0±39.3	18.1±54.5	18.1±53.9	17.2±56.9	15.7±53.3	17.1±57.7	14.7±51.5

Table 3: CS segmentation and pith estimation accuracy evaluation.

Real world verification performance Based on the PE accuracy evaluation P_{4SS} is selected for computing the geometric features in case of automated SEG/PE.

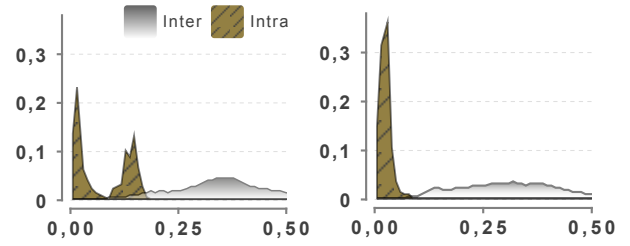
The verification performance results for all configurations are summarized in Table 1 and 2. Equal as for the GT-based configuration, the best EERs for each particular feature are achieved with the features E, PEC, RD and Z. It is astonishing that the Zernike moments show EERs that totally outperform the other features. In addition, the EERs computed with the automated configurations outperform the GT-based EER achieved with Z.

The intra- and interclass distribution for the best EER = 5.4% (SEG-C/PE-PEAK) and Zernike moments (Z) is depicted in Fig. 5a. The chart shows that the intraclass distribution is splitted into two parts. The left part belongs to intraclass distances between CS images with a high segmentation accuracy and the right part to distances between worse segmented CS images.

Regarding all EERs, except the HU features, the results in Table 2 show that using SEG-C improves all EERs compared to the SEG-G results. Furthermore, the SEG-G and SEG-C results show that the PE-PEAK approach achieves better EERs compared to the PE-PCA approach.

Beneath the Zernike moments, the radial pith and centroid distances (PD and CD) achieve the next best EERs. For all configurations PD performs better than CD. The best EER for PD and the automated configurations is achieved with SEG-C/PE-PEAK and accounts 15.2 %. Considering all configurations, it can be stated that HU moments are less suited as geometric CS features. The EERs for each particular feature indicate that the SEG-C/PE-PEAK configuration is the best for the computation of geometric features.

Finally, the fusion based EERs presented in Table 1 are assessed. For the GT-based configuration all fusion results lead to an improvement of the verification performance. The fusion of PD, CD, Z achieves an EER of 0.54% (see Fig. 5b). In case of the automated configurations Z is neglected because the fusion results were less interesting. However, just



(a) SEG-C/PE-PEAK: Zernike moments (Z) - EER=5.4% (b) GT: Fusion of PD, CD, Z - EER=0.54%.

Fig. 5: Selected intra-, interclass score distributions [X-Axis: Matching Score, Y-Axis: Probability]

for one configuration (SEG-C/PE-PCA) the fusion of PD, CD improves the best EER (16.6%) achieved with PD to 15.75%. For all other results feature fusion does not improve the EERs of the automated configurations.

4. CONCLUSION

This work assesses the discriminative power of geometric log end features and validates their reliability in case of performing automated CS segmentation and pith estimation. The experimental evaluation forms a solid basis for the further development of a biometric log recognition system.

In case of GT-data the verification performance evaluation showed that radial distances (CD, PD) and Zernike moments (Z) show a high discriminative power. Score level fusion of these features leads to an EER of 0.54%. The validation of these features for automated segmentation and pith estimation showed that Zernike moments achieve the highest reliability. Compared to Zernike moments the EERs for CD and PD are strongly influenced by automated segmentation and pith estimation.

Future work should investigate the fusion of the best geometric features with annual ring pattern features.

5. REFERENCES

- [1] W.A. Barrett, "Biometrics of cut tree faces," in *Advances in Computer and Information Sciences and Engineering*, Tarek Sobh, Ed., pp. 562–565. Springer Netherlands, 2008.
- [2] R. Schraml, J. Charwat-Pessler, and A. Uhl, "Temporal and longitudinal variances in wood log cross-section image analysis," in *IEEE International Conference on Image Processing 2014 (ICIP 2014)*, Paris, FR, Oct. 2014.
- [3] R. Schraml, J. Charwat-Pessler, A. Petutschnigg, and A. Uhl, "Robustness of biometric wood log traceability using digital log end images," Tech. Rep. 2014-08, Department of Computer Sciences, University of Salzburg, Austria, <http://www.cosy.sbg.ac.at/tr>, 2014.
- [4] A. K. Jain, S. Prabhakar, L. Hong, and S. Pankanti, "Filterbank-based fingerprint matching," *IEEE Transactions on Image Processing*, vol. 9, no. 5, pp. 846–859, May 2000.
- [5] A. Jain, A. Ross, and S. Prabhakar, "Fingerprint matching using minutiae and texture features," in *Procs. of the International Conference on Image Processing (ICIP'01)*, Thessaloniki, GR, 2001, vol. 3, pp. 282–285.
- [6] R. Schraml and A. Uhl, "Tree log identification based on digital cross-section images of log ends using fingerprint and iris recognition methods," Tech. Rep. 2015, Department of Computer Sciences, University of Salzburg, Austria, <http://www.cosy.sbg.ac.at/tr>, 2015.
- [7] R. Schraml and A. Uhl, "Pith estimation on rough log end images using local Fourier spectrum analysis," in *Proceedings of the 14th Conference on Computer Graphics and Imaging (CGIM'13)*, Innsbruck, AUT, Feb. 2013.
- [8] R. Schraml and A. Uhl, "Similarity based cross-section segmentation in rough log end images," in *Proceedings of the 10th Artificial Intelligence Applications and Innovations Conference (AIAI'14)*, L. Iliadis et al., Eds., Rhodes, GR, 2014, vol. 436 of *Springer IFIP AICT*, pp. 614–621.
- [9] I. Pitas, *Digital Image Processing Algorithms and Applications*, John Wiley & Sons, Inc., New York, NY, USA, 1st edition, 2000.
- [10] Ming-Kuei Hu, "Visual pattern recognition by moment invariants, computer methods in image analysis," *IRE Transactions on Information Theory*, vol. 8, 1962.
- [11] R. Mukundan and K. R. Ramakrishnan, *Moment Functions in Image Analysis: Theory and Applications*, chapter Zernike Moments, pp. 57–70, World Scientific Publishing Company, 1988.
- [12] Chee-Way Chong, P. Raveendran, and R. Mukundan, "An efficient algorithm for fast computation of pseudo-zernike moments," *International Journal of Pattern Recognition and Artificial Intelligence*, vol. 17, no. 6, pp. 1011–1023, 2003.
- [13] Anil K. Jain, Arun A. Ross, and Karthik Nandakumar, *Introduction to Biometrics*, Springer US, 2011.
- [14] P. Pudil, J. Novovičová, and J. Kittler, "Floating search methods in feature selection," *Pattern Recognition Letters*, vol. 15, no. 11, pp. 1119–1125, 1994.
- [15] Ruud M. Bolle, Nalini K. Ratha, and Sharath Pankanti, "Error analysis of pattern recognition systems: The subsets bootstrap," *Comput. Vis. Image Underst.*, vol. 93, no. 1, pp. 1–33, Jan. 2004.